Applied Catalysis B: Environmental 142–143 (2013) 432–441

Contents lists available at SciVerse ScienceDirect

Applied Catalysis B: Environmental

journal homepage: www.elsevier.com/locate/apcatb

Visible light assisted reduction of 4-nitrophenol to 4-aminophenol on Ag/TiO_2 photocatalysts synthesized by hybrid templates

Mohamed Mokhtar Mohamed[a,b,*], Merfat S. Al-Sharif[c]

[a] Umm Al-Qura University, Faculty of Applied Science, Chemistry Department, Makkah, Saudi Arabia
[b] Benha University, Faculty of Science, Chemistry Department, Benha, Egypt
[c] Al-Taief University, Faculty of Science, Chemistry Department, Al-Taief, Saudi Arabia

ARTICLE INFO

Article history:
Received 7 December 2012
Received in revised form 10 May 2013
Accepted 24 May 2013
Available online 30 May 2013

Keywords:
Photoreduction
p-Nitrophenol
Ag/TiO_2
Hybrid template
Characterization

ABSTRACT

Silver nanoparticles were successfully assembled in self-organized polyhedral TiO_2; synthesized by hybrid template consisting of pluronic-85, hexadecyltrimethylammoinm bromide and triethanol amine ($TPHtAg_2$), as well as in platelets TiO_2; synthesized only via hexadecyltrimethylammonium bromide ($THAg_2$). X-ray diffraction, transmission electron microscopy, X-ray photoelectron spectroscopy, diffuse reflectance UV–vis spectroscopy as well as N_2 sorptiometry were used for the characterization of phase composition, surface morphology, valent states of Ag/TiO_2, optical and surface texturing properties. These nanomaterials were tested as catalysts for 4-nitrophenol (4-NP) reduction in presence of aqueous $NaBH_4$ under visible-light irradiation. The results showed that the $THAg_2$ catalyst exhibited the best photocatalytic performance in the reduction of 4-NP into 4-aminophenol (4-AP) and revealed 98% conversion following 2 min irradiation with rate constant equal 0.025 s^{-1}. On the other hand, the $TPHtAgS_2$ catalyst, derived from using Ag_2SO_4 as a precursor instead of $AgNO_3$, indicates a conversion comprised of 80% at similar reaction conditions. The superiority of the photocatalytic reduction of $THAg_2$ was due to exposing Ag^+ ions together with Ag^0 nanoparticles (5 nm) and to the photo-induced role of carbon atoms; formed as a result of the non-complete decomposition of the template, and its synergistic effect with the anatase phase. On the contrary, $TPHtAg_2$ showed strong chemical interaction of Ag^+ ions within the hybrid templates and as a result inhibits the reduction of Ag^+ ion as well as the adsorption of 4-NP and eventually indicates no activity. The decreased activity and stability of $TPHtAgS_2$ compared with $THAg_2$ was due to increasing the particles size of Ag^0 (10 nm), diminishing the accessibility and reactivity of Ag^+ ions; which could have been worked as trapping sites with Ag^o, and the limited effect of residual S^{2-} ions, depicted from XPS measurements.

1. Introduction

Aromatic amines are important organic pollutants and are intermediates or side products of many industrial products such as dyes, pharmaceuticals, agro-chemicals, cosmetics, photographic chemicals and chelating agents [1–4]. The methodology of synthesizing organic functionality is important for the synthetic chemists to synthesize vital organic molecules. Thus, researchers tried to employ new techniques such as photocatalysis; one of the developing fields, via utilizing visible-light irradiation for instance to reduce organic functionality. The hydrogenation of a range of aliphatic [5] and aromatic [6] nitro-compounds in both gas [7,8] and liquid [9,10] phase processes, via metal/acid reduction and electrolytic reduction, is difficult to achieve in the presence of reactive substituents such as —Cl, —CH_3 and —OH. Great numbers of studies for the reduction of p-nitrophenol to p-aminophenol have been performed over the past few decades [11–13]. The catalytic liquid phase reaction using standard transition metals (e.g. Ni [14], Pd [15], and/or Pt [16]) exhibits limitations in terms of evoking unfavorable toxic secondary reaction products such as azo- [17] and/or azoxy-derivates [18].

In general, TiO_2 exhibits no hydrogenation activity relative to typical transition metal catalysts [19] because it suffers high recombination rate of charge carriers and the need for UV radiation to excite electron–hole pairs due to its large band gap (3.2 eV for anatase) [12–19]. Besides, the low quantum yields, particularly in the visible light range hinder its practical application. Many efforts have been attempted to enhance the absorption in the visible spectrum by tuning the band gap of TiO_2 through altering

* Corresponding author at: Umm Al-Qura University, Faculty of Applied Science, Chemistry Department, Makkah, Saudi Arabia. Tel.: +966 0500969808.
E-mail address: mohmok2000@yahoo.com (M.M. Mohamed).

0926-3373/$ – see front matter © 2013 Elsevier B.V. All rights reserved.
http://dx.doi.org/10.1016/j.apcatb.2013.05.058

preparation methods. A variety of strategies have been tried to prepare Ag deposited-TiO_2 materials, for instance, photodeposition, chemical deposition and conventional impregnation method [20]. In the earlier reports, most of the Ag–TiO_2 nanocomposites were composed of randomly mixed TiO_2 and Ag nanoparticles [21,22]. However, TiO_2 particles tend to agglomerate leading to decrease in surface area and phase separation during repeated utilization. Moreover, if the Ag nanoparticles cannot be well dispersed on the surface of TiO_2, the density of active sites on the Ag/TiO_2 surface will be low and thus affects the activity. It has been shown that incorporating Ag improved the photocatalytic efficiency of TiO_2-based photocatalyst [23,24] owing to the effective hindering of photoinduced electrons and holes from recombination. Moreover, the surface plasmonic resonance (SPR) effects of the Ag nanoparticles can red shift the absorption into visible light region [25]. Accordingly, in a way of synthesizing a potential catalyst capable of facilitating the photocatalytic reduction of 4-nitrophenol via visible-light irradiations, a highly dispersed Ag nanoparltices inside TiO_2 was synthesized by the one-pot technique via using hybrid templates to produce Ag nanoparticles embedded inside tailored mesoporous TiO_2 networks of controllable morphologies. The synthesized materials have been thoroughly characterized by XRD, TEM, N_2 sorptiometry, XPS and UV–vis diffuse reflectance spectroscopy. The reduction of silver ions in Ag/TiO_2 is carried out during the reduction process of 4-nitrophenol; to its corresponding 4-aminophenol, via employing $NaBH_4$. The progress of the reduction reactions was followed by UV–vis spectrophotometer.

2. Experimental

2.1. Assembly of Ag nanoparticles in TiO_2

TiO_2 nanoparticles were fabricated by self assembly method according to the following procedure. Briefly, pluronic-85 ($EO_{25}PO_{40}EO_{25}$-0.01 M) and hexadecyltrimethylammoinm bromide ($C_{16}H_{33}$)$N(CH_3)_3$Br-0.01 M) dissolved in a least amount of water (25 ml) in a weight ratio of 7:3 were mixed thoroughly for 1 h. To the previous mixture, 5 ml of triethanol amine was added and stirred for 0.5 h. Titanium iso-propoxide ($Ti(OCH(CH_3)_2)_4$-29.3 ml) was then added into the above mixture via a drop wise manner with vigorous stirring for 1 h at room temperature followed by adjusting the pH by HNO_3 solution (0.1 M) into 1. The resulting reaction mixture was transformed into an autoclave lined with Teflon followed by hydrothermal treatment at 373 K for 48 h. After hydrothermal treatment, the product was recovered by centrifugation and then washed 3 times with deionized water. The solid was then dried overnight at 393 K for 5 h and further calcined in air at 673 K for 6 h. This sample was denoted as TPHt, where the letters T, P, H and t refer respectively to titanium isopropoxide, pluronic-85, hexadecyltrimethylammoinm bromide and triethanol amine. $AgNO_3$ insertion took place at a ratio of 2 wt% simultaneously during the addition of titanium iso-propoxide to prepare samples denoted as $TPHtAg_2$. In the same way, Ag_2SO_4 was used instead of $AgNO_3$ to synthesize sample denoted as $TPHtAgS_2$; where AgS represents Ag_2SO_4 and 2 signifies the sample insertion ratio. On the other hand, the TH sample was simply synthesized by dissolving 0.036 g of hexadecyltrimethylammoinm bromide in 100 ml of 1 molar NaOH solution. To the later solution, 29.3 ml of Titanium iso-propoxide was added in a step-wise manner with continuous stirring till complete precipitation followed by adjusting the pH into 8. This mixture was left for two days followed by filtering, washing with water-ethanol, drying at 393 h for 5 h and finally calcining at 673 K for 4 h. $AgNO_3$ inclusion took place; at a ratio of 2 wt% simultaneously with the addition of titanium iso-propoxide to prepare samples denoted as $THAg_2$.TiO_2 P25 (80% anatase: 20% rutile) with a surface area of 49 m^2/g and primary crystal size 30 nm that purchased from Degussa was impregnated with $AgNO_3$ at a ratio of 4% to give a catalyst denoted as $P_{25}Ag_4$, for comparison purposes. Different patches were synthesized for the Ag/TiO_2 catalysts following up the same procedure and as a result a good reproducibility has been attained.

2.2. Physicochemical characterization of materials

2.2.1. X-ray diffraction analysis

X-ray diffraction analysis was performed on X-ray diffraction (XRD) spectrometer Model XRD 8030 from Jeol co., Japan. Maximum power is 3 kw and the unit is equipped with rotating stage and thin layer accessories. The patterns were run with Co-filtered Co Kα radiation (λ = 1.79 Å) energized at 45 kV, and 10 mA. The counter is scintillation with dead 10^{-6} s. The samples were measured at room temperature in the range of 2θ = 20 to 80°. The XRD phases present in the samples were identified with the help of ASTM Powder Data Files.

2.2.2. Transmission electron microscope (TEM)

The observation of the particle shape and the measurement of the particle size distribution of the precipitate was performed using a JEM-2100F transmission Electron Microscope (JEOL) via conductive carbon paint. The strength is 200 kV with 0.23 nm sensitivity.

2.2.3. Nitrogen adsorption measurements

Nitrogen adsorption measurements were performed at liquid nitrogen temperature with a Micromeritics ASAP 2020 surface area and porosity analyzer. Prior to the measurements, the samples were degassed for half an hour at 363 K followed by 3 h at 473 K. Surface area was calculated using the BET (Brunauer–Emmett–Teller) interpretation of the nitrogen adsorption isotherm. The pretreatment conditions must remain sufficiently mild to avoid any modification of the textural characteristics of the sample but severe enough to obtain a good surface clean-up.

2.2.4. Ultraviolet–visible diffuse reflectance spectroscopy

Diffuse reflectance ultraviolet–visible spectroscopy (UV–vis DRS) of powder catalyst samples was carried out at room temperature using a PerkinElmer Lamda-35 spectrophotometer in the range of 200–800 nm.

2.2.5. X-ray photoelectron spectroscopy (XPS)

X-ray photoelectron spectroscopy (XPS) measurements were taken on the Thermo Scientific Escalab 250Xi spectrometer with an MCD-9 detector and with a monochromatic XR6 source for XPS analyses. This offers a user-selectable spot size from 200 to 900 μm. Automated in-lens irises may also be used to reduce the analysis area further, offering a range of 300–20 μm. Spectra treatment was performed using the CASA software. All data were acquired in a single, unattended analysis. The dual ion/electron flood source charge neutralization system, using very low energy electrons and ions, was used for the analysis of insulating samples. Typically the hydrocarbon C1s line at 284.8 eV is used for energy referencing. All data processing (quantification, peak fitting, image generation, PCA, average spectrum generation etc.) was performed within the Avantage datasystem.

2.2.6. Activity measurements by catalytic reduction of 4-NP

To investigate the catalytic reduction of 4-NP (1.8×10^{-4} M), a 300 ml glass photoreactor equipped with Hg lamp; with a special UV cut off filter (λ = 420 nm) offering visible light source, was illuminated in presence of 1 g/l catalyst at 298 K together with injecting 5 ml of $NaBH_4$ of 2.0×10^{-1} M under constant stirring. The yellow color of solution gradually vanished, indicating the reduction of 4-NP, during the hydrogenation process. Samples were directly

Table 1
Crystallinity, particles size and lattice spacing of TiO_2 and Ag/TiO_2 synthesized using hybrid templates via self-assembly method.

Sample	%Crystalinity[a]		Particle[b] size (nm)	Lattice parameter (Å)			Lattice volume (Å^3)
	Anatase	Rutile		*a*	*b*	*c*	
TPHt	17.5	82.5	20	4.58		2.95	62.92
$THAg_2$	100	–	19	3.79		9.51	136.3
$TPHtAg_2$	7.5	92.5	20	4.58		2.95	62.92
$TPHtAgS_2$	21	79	24	4.58		2.95	62.92

[a] The mean fraction of rutile (X_r) and anatase in the crystal lattice is calculated respectively based on the relationship between the integrated intensities of anatase (1 0 1) and rutile (1 1 0) peaks using the formulas cited in references[19,21].
[b] The crystallite sizes of the resultant titania phases is estimated by the Scherrer's formula: $D(\text{hkl}) = K1\lambda/(\beta 1/2 \times \cos\theta)$.

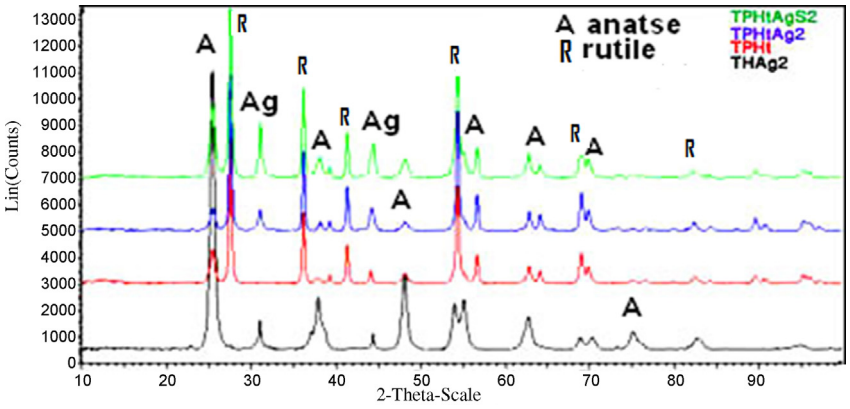

Fig. 1. XRD patterns of TPHt, $THAg_2$, $TPHtAg_2$ and $TPHtAgS_2$.

withdrawn from the reaction medium after certain regular interval irradiation time followed by measuring UV–vis; using a Hitachi U-3000 spectrophotometer, spectra of these solutions to monitor the decrease in intensity of the absorption peak at 400 nm for 4-NP. The rate constant of the reaction was determined by measuring the change in intensity of these peaks with time. The progress of the reaction and the activation parameters for the reduction reactions of 4-NP to the corresponding amine, 4-aminephenol, was determined. At the end of the reaction, the catalysts were separated from the suspension containing Ag/TiO_2 nanocatalysts and the product 4-aminophenol was also identified by capillary column gas chromatography (Varian 3900).

3. Results and discussion

3.1. XRD and TEM analysis

The results of XRD analysis of synthesized titania nanopowders derived from employing the hybrid template composed of H, P and t together with those incorporated with Ag ions (Table 1 and Fig. 1), confirm the findings of anatase (JCPDS 21-1272) as the minor phase and rutile (JCPDS 21-1276) as the major one. On the contrary, the sample formed as a result of employing Hexadecyltrimethylammonium bromide (H) as a sole template with Ag promotes 100% anatase only. A quantitative analysis of the phase composition of titania is performed by examining the XRD patterns by calculating the integrated intensities of anatase (1 0 1) and rutile (1 1 0) peaks [26]. The presence of the hybrid template promotes an anatase phase composed of 17.5% and a rutile phase at 82.5% in the TPHt sample. Incorporating Ag as $AgNO_3$ in the $TPHtAg_2$ sample at a loading of 2 wt% decreases the anatase percentages into 7.5 and enhances those of rutile into 92.5%. On the other hand, incorporating Ag as Ag_2SO_4 in the $TPHtAgS_2$ sample at similar loading (2%) increases the former ratio into 21% and decreases that of the latter into 79% highlighting the effect of Ag_2SO_4 on the transformation of the TiO_2 into the anatase phase. Achieving 100% anatase cyrstallinity in the $THAg_2$ sample concludes that both pluronic and triethanol amine motivate the formation of the rutile phase. Lattice constants of TiO_2 samples synthesized using H, P and t including $TPHtAg_2$, $TPHtAgS_2$ and TPHt presented similar values for a and c unit cell parameters and indicated lattice volume value comprised of 62.92 Å^3 (crystal structure rutile tetragonal, space group, $P4_2/mnm$). On the other hand, the $THAg_2$ sample undergoes a substantial change with lattice volume and enhances it into 136.30 Å^3 (crystal structure anatase tetragonal, space group, $I4_1/amd$) concluding that the anatase lattice is extended along the *c*-axis in case of CTAB surfactant and gives a clue about the probability of accumulating Ag^+ ions onto it. All the samples are of comparable crystallites size encompassing the margin from 19 to 20 nm except $TPHtAgS_2$ that exhibited crystallites size equal 24.0 nm. At 2 wt% Ag, a peak of varied intensity at 31.3° corresponding to Ag_2O of (2 1 1) is observed in the order $TPHtAgS_2 > THAg_2 > TPHtAg_2$ reflecting the lower dispersity of such species in the same order as well as decreasing the reduction capability of either p (PEO-PPO-PEO) and/or CTAB (H) to Ag^+ moieties. A diffraction peak at $2\theta = 38.3°$ was hardly recognized; due to interfering with that of anatase (at $2\theta = 37.8$), in $THAg_2$ due to Ag^0 (1 1 1) together with a diffraction peak corresponding to Ag^0 (2 0 0) at $2\theta = 44.2°$ for $THAg_2$, $TPHtAg_2$ and $TPHtAgS_2$ samples highlighting the presence of unlike Ag^0 nanoparticles of different origins. Increasing the intensity of the diffraction line at $2\theta = 44.2°$ rather than that at 38.3° reflects the exposure of the (2 0 0) facet rather than that of (1 1 1) on the surfaces of titania crystals. These reflection peaks can be indexed to face-centered cubic of metallic silver [27]. The preferential (2 0 0) orientation of Ag^0 neither depend on anatase rich sample ($THAg_2$) nor rutile rich ones ($TPHtAg_2$ and $TPHtAgS_2$). Accordingly, this let us conclude that some of Ag incorporated TiO_2 are in the reduced state as well as in Ag_2O state.

Fig. 2 shows the TEM image of TPHt that composed of clear crystals of polygonal structures containing mainly tetrahedral and pentahedral shapes. The average crystallites size was ranging from 16 to 40 nm with an average size of about 27 ± 3 nm. Parallel

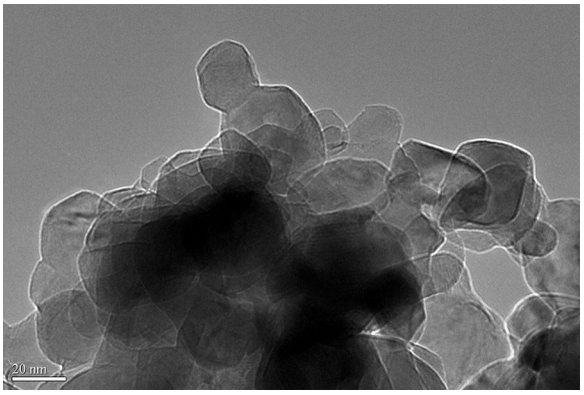

Fig. 2. TEM image of TPHt.

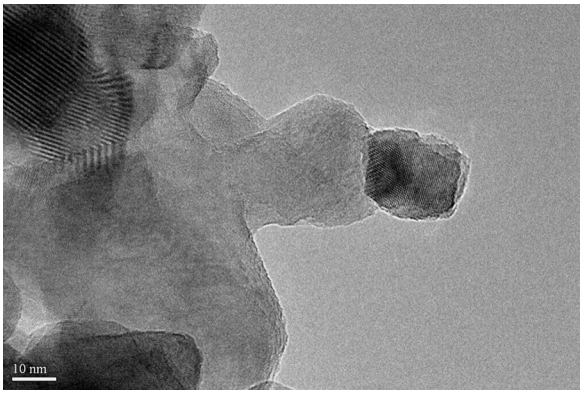

Fig. 3. High magnification TEM image of TPHt.

channels are observed upon magnification indicating the presence of ordered porous structure in the sample (Fig. 3). Lattice spacings characteristic of rutile phase at 0.324 nm (Fig. 3) together with those corresponding to the anatase phase at 0.356 nm are observed. This close interconnection between the two phases at the left side of the image was supposed to favor the photoinduced electrons transfer between the phases [28] that assume to reduce the recombination of the photoinduced electrons and holes, and improve the photocatalytic activity of the catalysts. $TPHtAg_2$ and $TPHtAgS_2$ catalysts show images similar to that of TPHt (not shown). Fig. 4 shows the TEM image of $THAg_2$ in which a homogeneously dispersed Ag nanoparticles of spherical morphology; of about 5 nm size, was

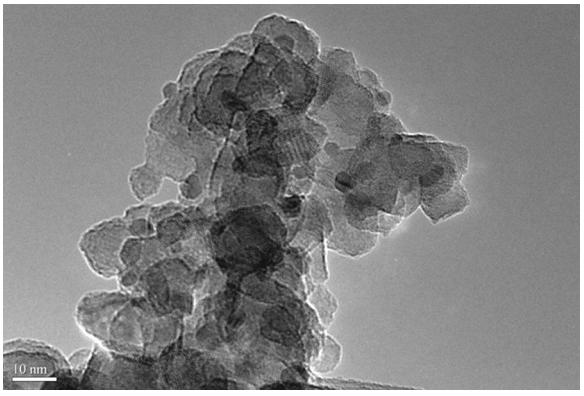

Fig. 4. TEM image of $THAg_2$.

localized and dispersed onto larger TiO_2 platelets-like structure. These later structures were highly aggregated and measure average sizes of 17 nm; comparable to those measured by XRD, signifying that Ag moieties have been incorporated into the pore channels of the TiO_2 structure; as devoted from surface texturing analysis illustrated in the coming section.

3.2. Surface texturing analysis

Fig. 5a and c shows the adsorption–desorption isotherms of $THAg_2$ and $TPHtAgS_2$ samples; as representative ones. They show large hysteresis loops characterizing mesoporous nature of H2 type, with cage like or ink bottle type of pores. It can be seen that the isotherms are never end at high pressures (till $P/P^0 = 1.0$) assuming macroporosity as well. The specific surface area and pore volume values illustrate a decrease in $THAg_2$ (39.7 m^2/g, 0.085 cm^3/g), $TPHtAgS_2$ (41.4 m^2/g, 0.11 cm^3/g) and $TPHtAg_2$ (35.4 m^2/g, 0.13 cm^3/g) samples compared to TPHt (53 m^2/g, 0.14 cm^3/g). This could give a hint on the localization of Ag moieties deep inside the pores affecting the pore volumes that by its turn decrease the surface area values. Accordingly, $THAg_2$ that presents the largest decrease in pore volume infers the high dispersity of Ag species, as confirmed from TEM investigation. In concordance, this sample indicates the lowest decrease in pore radius value that measures 7.7 nm (Table 2). Although $TPHtAgS_2$ and $THAg_2$ samples show similar hysteresis loops, the one related to $THAg_2$ was broader suggesting pore blocking effects in the $TPHtAgS_2$ sample. The pore size distribution determined by the BJH method is shown in Fig. 5b and d. The results showed that the pore size of $THAg_2$ was uniform in two different domain maximizing at 20 Å; as a broad band, and at 85 Å; as a sharp band, whereas that for $TPHtAgS_2$ showed a shift into 25 Å (broad) and 90 (broad) Å, respectively. This indicates that the Presence of pluronic, hexadecylammonium bromide and triethanol amine templates as well as hexadecylammonium bromide alone create ordered mesopores, however, the latter indicates higher margin of mesopores extended into 90 Å ($TPHtAgS_2$) comparable to that detected by *r* value (10 nm) seen in Table 2.

3.3. Diffuse reflectance spectroscopy

Fig. 6 depicts the diffuse reflectance spectra of synthesized catalysts calcined at 673 K. These spectra were noticeably different in the visible light region. One can see that the reflectance in the visible light region for $THAg_2$ indicates a red shift at 433 nm corresponding to an energy band gap of 2.86 eV. This value was lower than that of the standard commercial P25 Degussa (3.22 eV), indicating that the present self-assembly method using cetyltrimethylammonium bromide template permits the synthesis of a photoactive TiO_2 not only under UV-irradiation but also able to absorb an important quantity of photons from visible light. This change in the optoelectronic properties of TiO_2 can be attributed to a strong interaction between metallic center of TiO_2 and organic carbons deposited as a result of the non-complete decomposition of the surfactant moieties (H); as will be elaborated later using XPS investigations [29]. These interaction would induce a negative charge on TiO_2 surface [30] which enhance the charge transfer process from O^{-2} to Ti^{+4} responsible for the band-gap diminishing [31]. This surface interaction could be responsible for the enhancement of TiO_2 photoactivity in agreement with other works which propose the photoassist role of surface carbon species [32]. On the other hand, a blue shift is depicted upon incorporating Ag ions of different precursors with the template during synthesizing TiO_2 where Ag derived from Ag_2SO_4 shows a band at 419 nm (2.95 eV) and that of $AgNO_3$ shows a band at 405 nm (3.06 eV), confirming significant

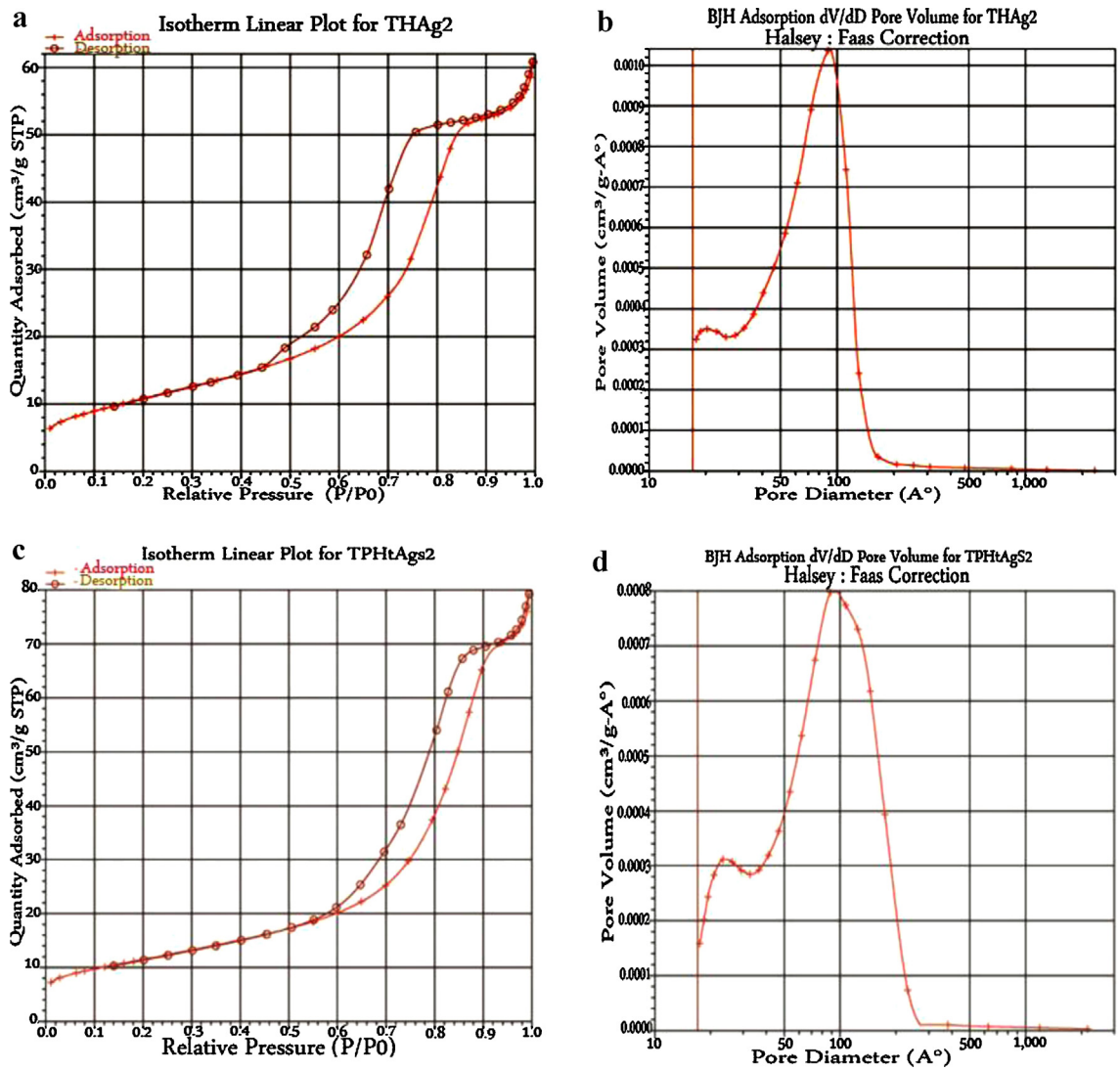

Fig. 5. (a) Isotherm linear plot for $THAg_2$. (b) BJH adsorption dV/dD pore volume for $TPHtAgs_2$. (c) Isotherm linear plot for $THAg_2$. (d) BJH adsorption dV/dD pore volume for $TPHtAgs_2$.

structural changes in the coordination environment of Ti species. For $TPHtAgS_2$, an additional plasmon resonance band characteristic of Ag nanoparticles at 580 nm is depicted together with a broad one at 700 nm. These bands are not consistent with the plasmonic absorption of AgNP used to be shown around 425 nm [33]. This thought to result from the aggregation of the AgNPs into larger sizes and to the presence of sulfur in the environment of Ti atoms [34]. This proposes that a non-uniform distribution of AgNPs with different sizes are present in this particular sample synthesized using silver sulfate that tend to form particles agglomeration, as depicted from TEM (not shown). Comparison with $THAg_2$ derived from $AgNO_3$ it did not indicate a band related to surface Plasmon resonance of Ag nanoparticles used to be around 425 nm probably due to overlapping with that evolved for TiO_2 at 433 nm. A shoulder at 350 nm was also discerned in this sample due to the anatase structure.

Table 2
Surface texturing properties of silver/titania nano-particles synthesized using hybrid templates via self-assembly method.

Sample name	[a] S_{BET} (m^2/g)	[b] S_t (m^2/g)	[c] V_p (cm^3/g)	[d] r (nm)	[e] S_{micro} (m^2/g)	[f] S_{meso} (m^2/g)	[g] V_{micro} (cm^3/g)	[h] V_{meso} (cm^3/g)
$THAg_2$	39.7	42.2	0.0858	7.7	–	–	0.0017	0.0841
TPHt	53	51.7	0.1453	9.6	1.32	51.68	0.0002	0.1451
$TPHtAg_2$	35.4	35.8	0.1314	12.1	–	–	0.0006	0.1308
$TPHtAgS_2$	41.4	39.8	0.1137	10	1.59	39.81	0.0004	0.1133

[a] S_{BET}; BET surface area.
[b] S_t; t-plot external surface area.
[c] V_p; pore volume.
[d] r; BJH adsorption average pore diameter.
[e] S_{micro}; t-plot micropore area.
[f] S_{meso}; mesopore area.
[g] V_{micro}; t-plot micropore volume.
[h] V_{meso}; mesopore volume.

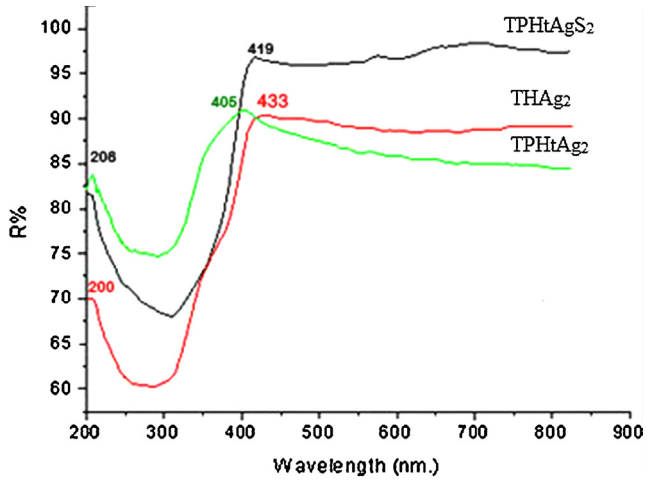

Fig. 6. Diffuse reflectance spectra of the catalysts $TPHtAg_2$, $TPHtAg_{S2}$ and $THAg_2$.

3.4. X-ray photoelectron spectroscopy

The surface composition and state of the products were further investigated using X-ray photoelectron spectroscopy. Fig. 7 shows the XPS spectra of $THAg_2$ and $TPHtAg_2$ as representative samples. The C 1s spectrum; depicted from $THAg_2$, showed a single strong peak at 284.6 eV and a weak one at 287.5 eV. Three forms of carbon species have been detected previously in literatures: elemental carbon (285 eV) located within the tetrahedral and octahedral interstices existing within the anatase crystal, Ti—C bond resulting from substituting oxygen atoms by carbon (287.5 eV), and carbonate species adsorbed on the surface (288 eV) [35]. Accordingly, most of the carbon incorporated in the TiO_2 matrix was present as elemental carbon, with small amounts of Ti—C species reside on the surface. XRD did not show any peaks for carbons suggesting that they are non-crystalline species. The XPS peaks indicate that the $THAg_2$ sample shows binding energies (BE) of Ti2p3/2 at 458.4 eV, which is in agreement with the reported literature values of Ti^{4+},[36] whereas that for $TPHtAg_2$ is shifted to 460.2 eV. This positive shift is attributed to enhancing the Ti—O—Ti linkage upon adding pluronic (tri-block copolymer) and triethanol amine to hexadecylammonium bromide. The O 1s binding energies of the pure TiO_2 derived from $THAg_2$ is located at 529.0 eV, due to the lattice O_2^- of TiO_2. The O 1s becomes broader with the pluronic template as in $TPHtAg_2$ and rather showed a shift in binding energy into 532 eV with the appearance of a shoulder at 533.5 eV infers from strengthening of Ti—O linkages. The later shift into 533.5 eV together with the decrease in the peak following Ag incorporation proposes the formation of Ag—O—Ti linkage. The two strong peaks at 368.0 and 370.2 eV for the Ag region depicted for $THAg_2$ and $TPHtAg_2$ respectively can be assigned to the binding energy of Ag 3d5/2, correlated to Ag^0 [37]. The shift of BE in the later compared to that of the former proposes a strong interaction of Ag^0 in $TPHtAg_2$ rather than within $THAg_2$. The absence of peaks at 367 and 367.7 eV due to AgO and Ag_2O, respectively could be related to the X-ray beam when hitting the sample affects surface silver oxide species converting them into metallic ones. On the other hand, in the $TPHtAgS_2$ sample (not shown) no carbon species were exposed on the surface; as on $TPHtAg_2$. The absence of carbons on the surface of these samples did not nullify their presence inside the surface as seen from narrowing their hysteresis loops compared with that of $THAg_2$. The higher shift of binding energies in the samples synthesized by the hybrid templates (P, H and T) reveals that the complexing effect of the head group of CTAB molecules with Ag^+ is weaker than that with the hybrid one.

3.5. Catalytic activity

In order to test the catalytic activity of the above mentioned characterized catalysts, the well-established catalytic reduction of 4-NP with $NaBH_4$ via visible-light irradiations is used and the progress of the reaction is followed spectrophotometrically. The conversion of 4-NP to 4-AP versus reaction time was only achieved for $THAg_2$ and $TPHtAgS_2$ catalysts (Fig. 8) whereas the rest of catalysts including TPHt, $TPHtAg_2$ and $P25Ag_4$ did not show any catalytic activity after 2 h reaction time. The good linear correlation of ln C_o/C versus time plot (Fig. 9) is the proof for the pseudo-first-order rate kinetics. As demonstrated, the reduction rate of 4-NP to 4-AP was completed in ~2.0 min irradiation exceeding 98% conversion whilst using the $THAg_2$ catalyst. It has been reported that the catalytic activity of nickel nanoparticles increased with the decrease in particles size during the conversion of 4-NP into 4-AP after 8 h reaction time [38]. Furthermore, the authors assessed that after the first 2 h reaction, an induction period was developed. This indicates to what extent the high-speed of our synthesized nanocatalysts in accomplishing the reduction compared with those of nickel ones as well as proceeding the reaction irrespective of the O_2 amount; dissolved in the aqueous medium, that compete with BH_4^- and 4-NP molecules via adsorption on Ag ions. Decreasing the particles size of TiO_2 in the $THAg_2$ catalyst into 17.0 nm compared with those of $THPtAgS_2$ (24.2 nm) reflect the effect of nanoparticles size on the catalytic activity. In particular, the former catalyst indicates highly dispersed Ag^0 (5 nm) nanoparticles on its surface than those on the later those presented average particles size of 10 nm. Smaller metal particles possess higher redox potential, thus facilitating electrons transfer [39]. Increasing the crystallinity percentages of anatase phase into 100% in $THAg_2$ did not prove that the anatase phase has a large influence on the activity because $THPtAgS_2$ showed an activity comprised of 80% although it owns only 21% anatase phase. In conformity, the $P25/Ag_4$ did not show any activity although it contains 80% anatase and since we know that the activity of P25 is negligible under visible irradiation, a run under UV-irradiation has been performed to indicate no activity as well proving that anatase could only give stability for Ag nanoparticles.

The catalysts were stirred in the 4-NP solution in the dark for 0.5 h to verify the extent of adorability of 4-NP on the catalyst surfaces prior to irradiation. It has been revealed that the $THAg_2$ sample showed an adsorption percentages comprised of 8%; in the absence of $NaBH_4$, whereas the rest of samples show negligible adsorption. Accordingly, increasing the activity of $THAg_2$ comparatively could be due to the synergistic effect of the TiO_2 anatase those accompanied with carbonaceous materials; as confirmed from XPS investigations. This was in conformity with the results demonstrated that the presence of carbon enhances the adsorption of organics and importantly the favorable adsorption on anatase rather than on rutile [36,39]. In addition, it seems that the anatase phase gives stability; as confirmed by many works, where rutile phase is generally less active due to lower surface affinity for many organic compounds and expected high rates of recombination of photogenerated charge pairs [40]. It has been depicted also that the presence of carbon within titania structure suppresses anatase–rutile transformation beside its effect on lowering the E_g value, as seen for $THAg_2$. Incorporating carbonaceous residues within titania substrates may also enhance TiO_2 photocatalytic activity by acting as a photosensitizer, transferring electrons to the TiO_2. This may be responsible for extending TiO_2 photocatalytic activity into the visible light range [41,42]. Thus, the photogenerated electron in the carbon is transferred into the conduction band of the TiO_2, assisting the reduction process. Lowering the catalytic activity of $TPHtAgS_2$ comparatively with time could also be due to the drop in the porosity and blockage of the photoactive centers

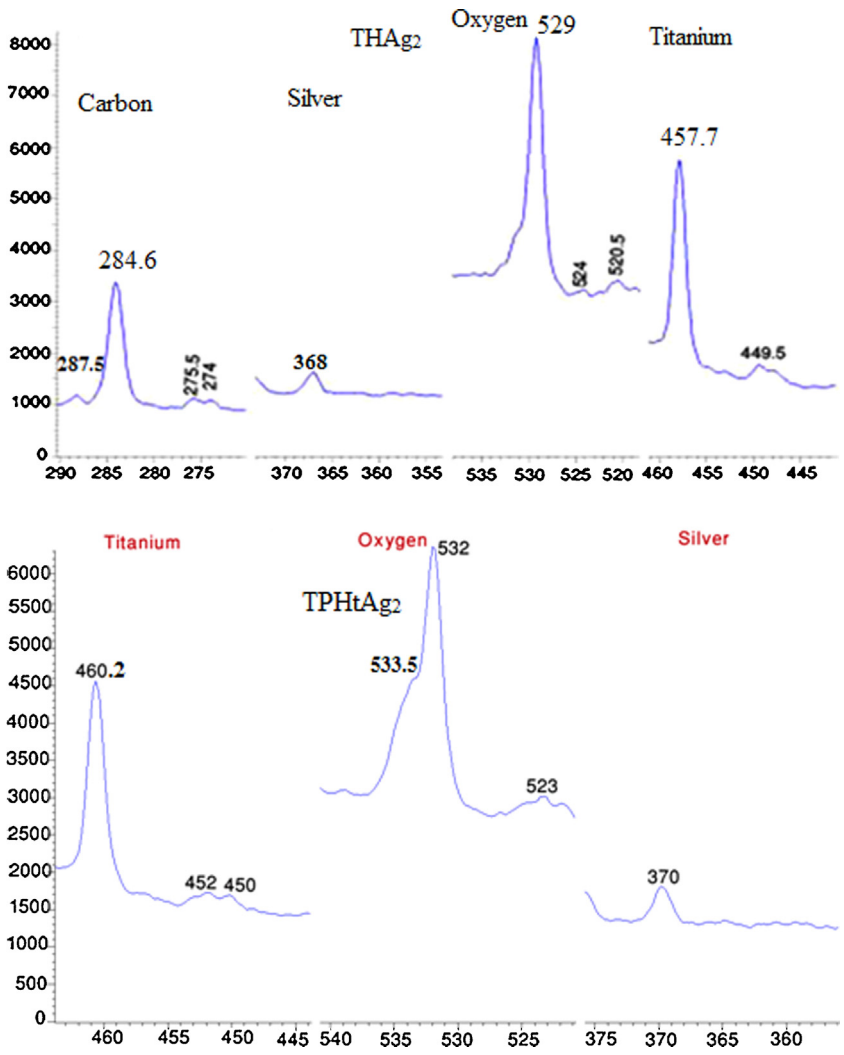

Fig. 7. XPS spectra of O 1s, C 1s, Ag 3d, and Ti 2p core levels for $THAg_2$ and $TPHtAg_2$ annealed at 673 K.

of the produced TiO_2 catalyst, as seen from the surface texturing results. The reduction reaction rate constants at 25 °C for 4-NP was 0.025 and 0.003 s^{-1} for $THAg_2$ and $TPHtAgS_2$, respectively, obeying pseudo first order rate kinetics. In other words, we propose that the origin of photocatalytic activity under visible light is due to a direct optical charge transfer transition involving both TiO_2 and carbons, keeping the high reactivity of the photogenerated electrons and holes. The reduction process occurs only under visible irradiation (light on) where no any change is revealed under the dark condition (light off).

It has been shown that in a photo-assisted reductive dehalogenation reaction, borohydride does not behave as a hydride donor instead it serves as a single electron and hydrogen atom donor [43]. This proves that the present catalytic process is only maintained by the excited state of the catalyst, which makes it to act as a photoredox catalyst. This experiment is highly helpful to understand about the light-responsive behavior of the catalyst. It is believed that the photoredox effects of the existing photocatalyst and its intelligence response toward the visible-light are unique. Such a light recognizing behavior makes the catalyst as a smart material, which may find superior use in the field of applied photo-technology [44].

We also conducted control experiments in which 4-NP solution was irradiated in the absence of any catalysts to exhibit no photolytic products were released. Mohamed and Al-Sharif [45] proposed that the reduction of 4-NP to 4-AP using $NaBH_4$ as the reducing agent is negligible if it is performed without using the catalyst. As can be seen from Fig. 10, a broad characteristic band at λ_{max} = 400 nm due the absorption of the 4-NP and $NaBH_4$ mixture is developed. When $THAg_2$ and $TPHtAgS_2$ are employed for the

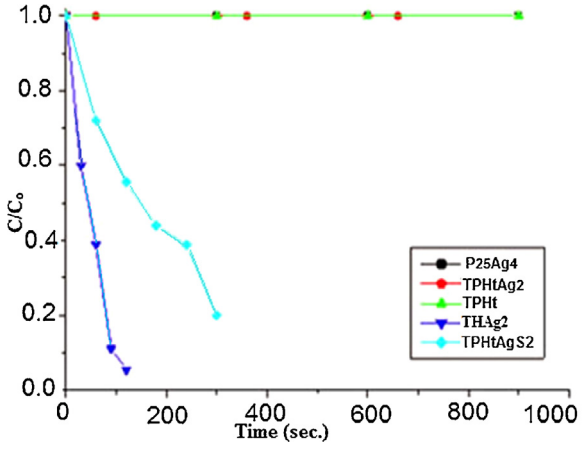

Fig. 8. The change in the concentration of 4-NP with time during reduction by TPHt, $THAg_2$, $TPHtAgs_2$, $TPHtAg_2$ and $P_{25}Ag_4$ catalysts in the presence of aqueous $NaBH_4$ (Reaction conditions: 100 ml [4-NP] = 1.8×10^{-4} mol/l, [$NaBH_4$] = 2.0×10^{-1} mol/l, 100 mg catalyst, 750 rpm.).

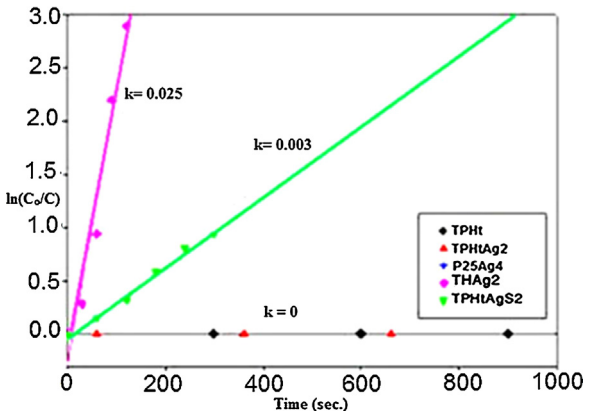

Fig. 9. ln C_o/C vs time of graph 8. (Reaction conditions: 100 ml [4-NP] = 1.8×10^{-4} mol/l, [$NaBH_4$] = 2.0×10^{-1} mol/l, 100 mg catalyst, 750 rpm.).

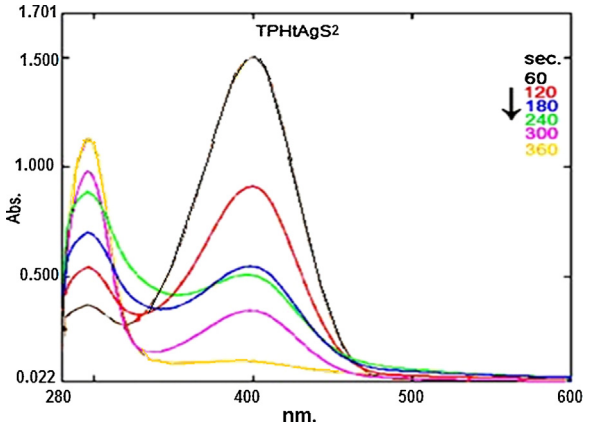

Fig. 10. UV–vis absorption spectra for the reduction of 4-NP over $TPHtAgs_2$ with an excess amount of $NaBH_4$ in aqueous media at 295 K.

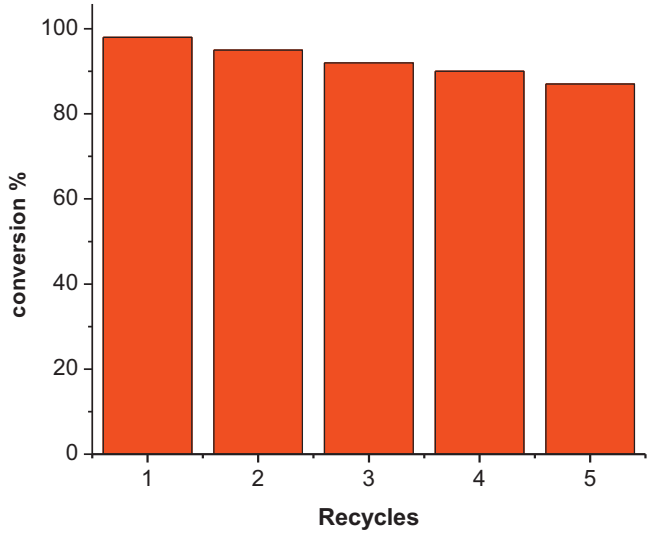

Fig. 11. Repeated cycles up to 5 times illustrating the conversion yield of 4-NP after 10 min over the $THAg_2$ photocatayst. The experimental conditions were kept constant at the following Reaction conditions: 100 ml [4-NP] = 1.8×10^{-4} M, [$NaBH_4$] = 2.0×10^{-1} M, 100 mg catalyst).

reduction reaction, a new band develop at λ_{max} = 293 nm representing the formation of 4-AP is built-up. The development of new peaks accompanies flattening the characteristic band at λ_{max} = 400 nm, indicating the reduction of 4-NP.

It has been proposed [46] that there were two steps of 4-NP reduction; (i) diffusion and adsorption of 4-NP to the Ag surfaces and (ii) electron transfer mediated by Ag surfaces from BH_4^- to 4-NP i.e. the electron transfer occurs from the negatively charged BH_4^- to the 4-NP via the AgNPs. $THAg_2$ had lower pore radius (7.7 vs. 12.1 nm) and pore volume (0.085 vs. 0.131 cm^3/g) values than $TPHtAg_2$, leading to the hard diffusion of 4-NP to Ag surfaces comparatively and thus the catalytic activity of $THAg_2$ did not depend on the diffusion step on which the reduction rate can count on but rather takes place on the surface. The electron transfer process depends upon the number of particles present in the solution as well as the available surface area of the catalyst particles [47]. It has been reported that [48] the reaction rate increases with an increase in the number of particles responsible for activating the reaction. Thus, the slightly faster reaction of $THAg_2$ (particle size 5 nm) than that of the $TPHtAgS_2$ (particle size 10) can be due to an increase in the d-electron density of the Ag atoms for the former comparatively, and thus leads to an increased reactivity to hydrogen atoms.

The proposed mechanism for the reduction of 4-NP by borohydride in the presence of AgNPs is given in Scheme 1a and b. The catalytic reduction proceeds on the surface of the metal nanoparticles. Decreasing the diameter of Ag nanoparticles (5 nm) that possess high redox potential; and thus may increase electron transfer, as well as increasing the ionic radius of Ag^+ (1.26 Å) than that of Ti^{4+} ion (0.67 Å); and as a result most of Ag will be localized at the surface, an expected charge transfer will be faster than the diffusion for the Ag nanoparticles-catalyzed the reduction reaction. In this scheme, two different routes are proposed for both $THAg_2$ and $TPHtAg_2$ catalysts. In the former one, the chemical interaction between Ag^+ and the surfactant counter ion to form $CTABr^-\cdots Ag^+$ complex is attained [49]. The latter complex can facilitate the reaction with the oxygen atom of the nitro group in 4-NP and consequently react with the borohydride ions, to form the metal hydride on the surface of AgNPs. Concomitantly, the adsorption of 4-NP on the AgNPs surface and evolution of 4-AP is attained overcoming the kinetic barrier of the reaction that facilitated as well via the bond with oxygen in O—Ti that decreases the partial positive charge on Ag^+; causing it reduction into Ag^0, due to the large electronegativity of O atom. In the case of $TPHtAg_2$, which give zero activity, the localized lone pair of electrons on the nitrogen of triethanol amine stabilizes the positive charge of Ag^+ ions; as devoted from XPS results, that in the same time attached from the other side to the Br^- ions of the CTAB molecule. Accordingly, the +ve charge on Ag will strongly interact with the −ve charge of oxygen atom in the NO_2 group of 4-NP and thus prohibited the reduction process of Ag^+ by $NaBH_4$ and thus block the reduction of nitro into the corresponding amino derivative. Such strong interaction of Ag^+ ion from both sides did not assist the adsorption of 4-nitrophenolate ions and thus did not help to overcome the kinetic barrier of the reaction. However in the case of $TPHtAgS_2$; which indicate conversion comprised of 80%, the probability of alcohol groups of triethanol amine to interact with S forming H_2S is very liable and thus freeing Ag^+ ions from the cage might have been formed because of triethanol amine extended arms. In conformity, no residual sulfur has been depicted using XPS technique. In addition, increasing the electronegativity of N atom of triethanol amine decreases the residual +ve charge on silver ion and thus facilitating the interaction with NO_2 group of 4-NP assisting its reduction via $NaBH_4$ together with simultaneous reduction of Ag^+ to eventually produce 4-AP moieties. In the same time the lager Ag_2SO_4 moieties compared with $AgNO_3$ ones, a given space to Ag^+ ion to interact is attained comparatively.

To explore the advantage of the $THAg_2$ catalyst and its applicability, reuse cycles of newly catalysts was tested for the reduction of 4-NP (Fig. 11). Experiments were performed where the catalyst

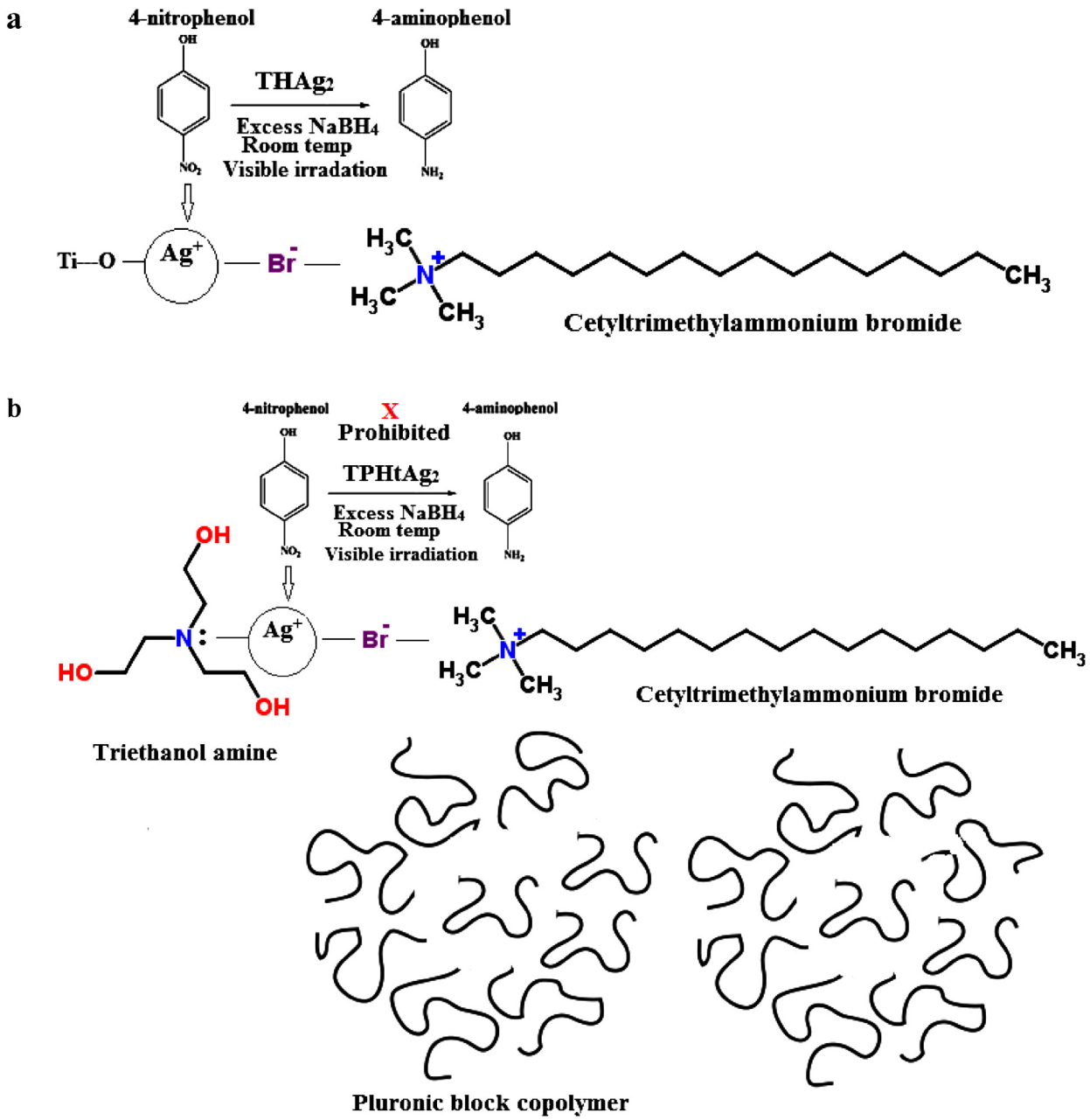

Scheme 1. The proposed mechanism of the reduction of nitro compounds by borohydride using $THAg_2$ catalyst (a) and (b) $TPHtAg_2$ catalyst in the presence of metallic AgNPs.

$THAg_2$ was recovered and reused by keeping all other parameters constant. The results revealed that $THAg_2$ shows a very good activity for five catalytic runs with a very small loss in the 4-NP conversion. The conversion yield of 4-NP after 10 min was still as high as 89% even at the fifth run. It can be conclude that the $THAg_2$ photocatalyst possesses reasonable stability and it may be reusable for at least 5 runs, showing a good potential for practical applications.

4. Conclusions

Assembly of Ag nanoparticles onto TiO_2 of platelets shape was successfully synthesized by one pot method employing hexadecylammoniumm bromide as template under hydrothermal conditions. This catalyst ($THAg_2$) has shown the best photoreduction performance (98% conversion in 2 min) when compared with $TPHtAg_2$; that gives zero activity, and $TPHtAgS_2$; that gives 80% conversion, those synthesized by the hybrid template due to the following aspects: (1) the well dispersion of Ag nanoparticles (5 nm) that works as the main hydrogenation site on the surface of TiO_2 of platelets morphology; (2) exposing residual carbons on the mesoporous anatase TiO_2 (100%) surface facilitate the enhanced photoreduction activity under visible light irradiation based on the electronic interaction between them. The rational design of hybrid Ag/TiO_2 nanostructures based on the employed hybrid templates including H, P and T raised some problems established in the chemical strength offered to Ag^+ ions during the synthesis with T and H molecules those offered difficulty in either the facile reduction of Ag^+ and/or the adsorption of 4-NP to give 4-AP. The absence of surface carbons on the catalysts synthesized by the hybrid template affects greatly the activity beside the dominance of the rutile phase did not stabilize Ag nanoparticles as anatase did.

Appendix A. Supplementary data

Supplementary data associated with this article can be found, in the online version, at http://dx.doi.org/10.1016/j.apcatb.2013.05.058.

References

[1] A. Saha, B. Ranu, J. Org. Chem. 73 (2008) 6867–6874.
[2] A. Rahman, S.B. Jonnalagadda, Catal. Lett. 123 (2008) 264–272.
[3] F. Cardenas-Lizana, S. Gomez-Quero, M.A. Keane, Catal. Commun. 9 (2008) 475–480.
[4] A. Vass, J. Dudas, J. Toth, R.S. Varma, Tetrahedron Lett. 42 (2001) 5347–5351.
[5] S.G. Harsy, Tetrahedron 46 (1990) 7403–7409.
[6] Y. Zheng, K. Ma, H. Wang, X. Sun, J. Jiang, C. Wang, R. Li, J. Ma, Catal. Lett. 124 (2008) 268–273.
[7] Z. Liu, X. Wang, H. Wu, C. Li, J. Colloid Interface Sci. 287 (2005) 604–610.
[8] V. Vishwanathan, V. Jayasri, P.M. Basha, N. Mahata, L.M. Sikhwivhilu, N.J. Coville, Catal. Commun. 9 (2008) 453–458.
[9] X.D. Wang, M.H. Liang, J.L. Zhang, Y. Wang, Curr. Org. Chem. 11 (2007) 299–307.
[10] B. Coq, F. Figueras, Coord. Chem. Rev. 178–180 (1998) 1753–1760.
[11] K.R. Westerterp, E.J. Molga, K.B. van Gelder, Chem. Eng. Process. 36 (1997) 17–24.
[12] H.W. Shih, M.N. VanderWal, R.L. Grange, D.W.C. MacMillan, J. Am. Chem. Soc. 132 (2010) 13600–13603.
[13] H. Lu, H. Yin, Y. Liu, T. Jiang, L. Yu, Catal. Commun. 10 (2008) 313–318.
[14] K.S. Shin, J.Y. Choi, C.S. Park, H.J. Jang, K. Kim, Catal. Lett. 133 (2009) 1–7.
[15] N. Yao, J. Chen, J. Zhang, J. Zhang, Catal. Commun. 9 (2008) 1510–1516.
[16] G. Zhang, L. Wang, K. Shen, D. Zhao, H.S. Freeman, Chem. Eng. J. 141 (2008) 368–373.
[17] K. Zhang, Y. Luo, Z. Li, Soft Mater. 5 (2007) 183–189.
[18] A. Corma, P. Serna, Science 313 (2006) 332–338.
[19] N.S. Chaubal, M.R. Sawant, J. Mol. Catal. A: Chem. 261 (2007) 232–239.
[20] Y. Mei, Y. Lu, F. Polzer, M. Ballauff, Chem. Mater. 19 (2007) 1062–1069.
[21] Y. Lu, Y. Mei, R. Walker, M. Ballauff, M. Drechsler, Polymer 47 (2006) 4985–4991.
[22] Y. Wang, G. Wei, F. Wen, X. Zhang, W. Zhang, L. Shi, J. Mol. Catal. A 280 (2008) 1–8.
[23] L. Liu, B. Qiao, Y. Ma, J. Zhang, Y. Deng, Dalton Trans. 19 (2008) 2542–2549.
[24] Y. Chen, C. Wang, H. Liu, J. Qiu, X. Bao, J. Chem. Soc., Chem. Commun. 42 (2005) 5298–5301.
[25] J. Ning, J. Xu, J. Liu, H. Miao, H. Ma, C. Chen, X. Li, L. Zhou, W. Yu, Catal. Commun. 8 (2007) 1763–1768.
[26] M.M. Mohamed, I. Othman, R.M. Mohamed, J. Photochem. Photobiol. A: Chem. 191 (2007) 153–162.
[27] X. Jiang, Y. Xie, J. Lu, L. Zhu, W. He, Y. Qian, Langmuir 17 (2001) 3795–3801.
[28] L. Ren, Y.-P. Zeng, D. Jiang, Catal. Commun. 10 (2009) 645–650.
[29] X. Zhang, M. Zhou, L. Lei, Mater. Chem. Phys. 91 (2005) 73–81.
[30] B. Zhao, Y.-W. Chen, J. Phys. Chem. Solids 72 (2011) 1312–1320.
[31] M.M. Mohamed, M. Al-Esaimi, J. Mol. Catal. A 255 (2006) 53–61.
[32] M. Abdulla-Al-Mamun, Y. Kusumoto, T. Zannat, Md S. Islam, Appl. Catal. A 398 (2011) 134–142.
[33] M.M. Mohamed, K.S. Khairou, Micropor. Mesopor. Mater. 142 (2011) 130–139.
[34] N.S. Chaubal, M.R. Sawant, J. Mol. Catal. A 261 (2007) 232–240.
[35] C. Oliveira, R.E. Galindo, C. Palacio, S. Calderon, B.G. Almeida, M. Henriques, A. Espinosa, S. Carvalho, Solid State Sci. 13 (2011) 95–101.
[36] G. Mul, A. Zwijnenburg, B. van der Linden, M. Makkee, J.A. Moulijn, J. Catal. 201 (2001) 128–136.
[37] J.H. Pan, H. Dou, Z. Xiong, C. Xu, J. Ma, X.S. Zhao, J. Mater. Chem. 20 (2010) 4461–4468.
[38] P.V. Suraja, Z. Yaakob, N.N. Binitha, M.R. Resmi, P.P. Silija, Chem. Eng. J. 176–177 (2011) 265–271.
[39] J. Liu, G. Qin, P. Raveendran, Y. Ikushima, Chem. Eur. J. 12 (2006) 2131–2138.
[40] M.M. Mohamed, B.H.M. Asghar, H.A. Muathen, Catal. Commun. 28 (2012) 58–63.
[41] C. Feng, J. Zhang, R. Lang, Z. Jin, Z. Wu, Z. Zhang, Appl. Surf. Sci. 257 (2011) 1864–1870.
[42] T. Ishida, K. Kuroda, N. Kinoshita, W. Minagawa, M. Haruta, J. Colloid Interface Sci. 323 (2008) 105–112.
[43] M. Cropp, G.B. Schuster, Tetrahedron Lett. 28 (1987) 5295–5298.
[44] S. Gazi, R. Ananthakrishnan, Appl. Catal. B 105 (2011) 317–325.
[45] M.M. Mohamed, M.S. Al-Sharif, Mater. Chem. Phys. 136 (2012) 528–537.
[46] N.C. Sharma, S.V. Salui, S. Nath, J.G. Parsons, J.L. Gardea-Torresde, T. Pal, Environ. Sci. Technol. 41 (2007) 5137–5142.
[47] K. Kuroda, T. Ishida, M. Haruta, J. Mol. Catal. A 298 (2009) 7.
[48] S. Kundu, S. Lau, H. Liang, J. Phys. Chem. C 113 (2009) 5150–5156.
[49] X. Li, J. Shen, A.D.Z. Zhang, G. Gao, H. Yang, J. Wu, Colloids Surf. A 400 (2012) 73–79.